

Capacitance and Force Computation due to Direct and Fringing Effects in MEMS/NEMS Arrays

Prashant N.Kambali and Ashok Kumar Pandey

Abstract—An accurate computation of electrical force is significant in analysing the performance of micro and nanoelectromechanical systems. Many analytical and empirical models are available for computing the forces, especially, for a single set of parallel plates. In general, these forces are computed based on the direct electric field between the overlapping areas of the plates and the fringing field effects. Most of the models, which are based on direct electric field effect, considers only trivial cases of fringing field effects. In this paper, we propose different models which are obtained from the numerical simulations. It is found to be useful in computing capacitance as well force in simple and complex configurations consisting of an array of beams and electrodes. For the given configurations, the analytical models are compared with the available models and numerical results. While the percentage error of the proposed model is found to be under 6% with respect to the numerical results, the error associated with the analytical model without the fringing field effects is around 50%. The proposed model can be applied to the devices in which the fringing field effects are dominant.

Index Terms—Electrostatic force, Fringing force, MEMS, NEMS, Capacitance, Arrays.

I. INTRODUCTION

Transduction in microelectromechanical systems (MEMS) or nanoelectromechanical systems (NEMS) is mainly based on electrostatic excitation. Electrostatic forces in these devices are found on the approximation of parallel plate capacitance with or without fringing effects. As the dimension of the devices reduces from micro to nanoscale, the fringing effect plays an important role [1]. The accuracy of the fringing force effects become even more important when an array of micro/nano beams operate in a cluster [2], [3] with or without bottom electrodes as shown in Figure 1. Since the electrostatic forces are obtained from the capacitance, we focus on the accurate formulation of capacitance in our analysis in different cases.

Figure 1(a) is one of the idealized parallel plates capacitor separated by a distance d apart. For a beam of length L , width b and the thickness h , the capacitance is given by $C_b = \epsilon_0 bL/d$ [4], where, $\epsilon_0 = 8.854 \times 10^{-12}$ F/m is the permittivity of the free space. However, if the beam is positioned at a distance of g from the side electrode as shown in Figure 1(b), then the capacitance is given by $C_s = \epsilon_0 hL/g$. For a case described in Figure 1(c) in which the beam is separated from the bottom and the side electrodes by distance d and g , respectively, the capacitance is given by $C = C_b + C_s$. It is to be noted that the

fringing effects are neglected for the cases described in Figures 1(a), (b), and (c). Therefore, we term the capacitance obtained in these cases as that due to the direct effect. When the fringing effects become significant, as described in Figures 1(d) and (e), in which the width of the bottom electrode and side electrode are greater than the width of the beam, respectively, it should be considered in the overall capacitance. For the beam under the extended bottom electrode, the capacitance is widely computed by [4], [5]

$$C = 2\pi\epsilon_0 \left[\ln \left(\frac{R + r + \sqrt{(R + r)^2 - r^2}}{r} \right) \right]^{-1} \quad (1)$$

where, $r = b/2$, and $R = d$ for the case shown in Figure 1(d). However, when the beam and side electrodes form different configurations with or without extended bottom electrode as shown in Figures 1(e)-(j), there are hardly any accurate formulation of capacitances in the literature.

To model the forces under different configurations of beam and electrodes, most of the study either uses the idealized case or some approximate empirical model. For example, to model the electrostatic forces in the dynamic pull-in analysis of a fixed-fixed microbeam, Nayfeh *et al* [6] used the direct electrostatic force model without considering the fringing effects. Gutschmidt and Gottlieb [7] studied the in-plane parametric vibration of an array of fixed-fixed beams based on the electrostatic model without the fringing field effects. Isacson *et al* [3] described the transverse and the longitudinal parametric resonances of carbon nanotube arrays with the electrostatic forces, formulated based on the charge distribution at the end of tubes. Recently, Hu *et al* [8] studied pull-in voltages of a micro curled beam under the effect of electrostatic force with the fringing field effects based on the formulation in [9]. Dumitru *et al* [10] also analyzed the transverse vibration of a microcantilever beam with bottom electrode including the first order correction for the fringing effect. Linzon *et al* [11] also studied the parametric response of a cantilever beam under the influence of fringing forces from the side electrodes. They obtained the forces by approximating the numerically obtained forces from the Intellisuite [12]. To improve the modeling of fringing effects in parallel plate capacitance, Palmer [13] used Schwartz-Christoffel conformal mapping transformation to evaluate the capacitance. Their model is used by Chang [14], Yuan *et al* [15] and Hosseini *et al* [16] to model fringing field effects in different problems. Chew and Kong [17] formulated the fringing effects based on the dual integral equations for circular microstrip disk. Slogget *et al*. [18] proposed higher order approximate formulas for capacitance based on the nu-

Prashant N.Kambali and Ashok Kumar Pandey are with the Department of Mechanical and Aerospace Engineering, Indian Institute of Technology, Hyderabad 502205, India (e-mails: me12p1004@iith.ac.in; ashok@iith.ac.in).
Manuscript received October 2014;

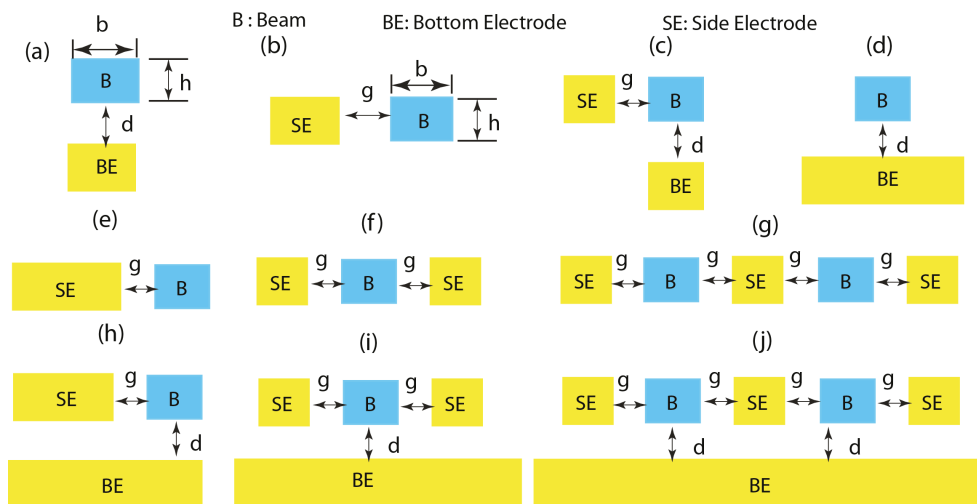


Fig. 1. Different configurations consisting of the beam, side electrode and the bottom electrode with and without fringing effect.

numerical simulation to capture fringing effects in parallel plate disc capacitors. Most of these models involve the correction for a single set of parallel capacitor. To model the capacitance for multi-strip lines over the ground electrode, Sakurai and Tamaru [9] proposed simple approximate expressions based on the numerical solutions for one, two, and three VLSI lines, respectively. However, the accuracy of their model is limited to a very simple case of thin wires. Moreover, the application of their formula to compute capacitance in an array of higher number of beams and electrodes have not been generalized. In this paper, we systematically propose an empirical formulation for the capacitance and force in a simple case of a beam and bottom electrode and also a beam and side electrode based on the numerical solution from the COMSOL [20]. After validating the formula with the available models, we generalize it to compute capacitance and forces in an array of different configurations of beams and electrodes. We also compare the results from the proposed formula with the numerical solution and the available model for a cantilever type of boundary condition.

II. NUMERICAL PROCEDURE FOR COMPUTING CAPACITANCE

In this section, we briefly describe the procedure for computing capacitance using COMSOL multiphysics software [20]. To make a model, we consider a cantilever beam of length L , width b , thickness h which is separated from the bottom electrode by a distance d as shown in Figures 2(a) and (b). One end of the beam is fixed and other end is free to have a cantilever type of boundary conditions. To capture the correct fringing field effects, we sufficiently extend the side boundaries and the top boundary of the surrounding air around the beam as shown in Figures 2(a) and (b). The mechanical and electrical properties of the beam can be prescribed as that of a Polysilicon having the Young's modulus of 153 GPa, the density as 2330 kg/m³, the Poisson's ratio of 0.23, and the relative permittivity of 4.5. To find the capacitance, we use electromechanics interface to solve the coupled equation governing structural deformation and electrostatic field under

the static equilibrium of the beam in the defined domain as shown in Figure 2(c). For the static analysis, a voltage of 1 V is applied to the beam and 0 V is applied to the bottom electrode, the potential V and electric field E , in the free space can be obtained by solving the following equations [20]:

$$\nabla \cdot (\epsilon \nabla V) = 0, \text{ and } E = -\nabla V.$$

If the total charge is Q and the voltage difference between the beam and the electrode is V , then the capacitance is given by

$$C = \frac{|Q|}{V}, \text{ where, } Q = \int_v (\nabla \cdot \epsilon E) dv$$

where, ϵ is relative permittivity, $\epsilon = 1$ for the surrounding air.

A. Numerical validation

TABLE I
 COMPARISON BETWEEN NUMERICAL RESULTS WITH RESPECT TO THE STANDARD ANALYTICAL MODELS FOR COMPUTING CAPACITANCE FOR CONFIGURATIONS SHOWN IN FIGURE 1(A),(B) AND (C).

Cases	Dimensions (μm)			Capacitance without fringing		% diff $\frac{N-A}{N} \times 100$
	g	d	h	Anal. Soln. (A) Farad (F)	Num. Soln. (N) Farad (F)	
(a)	—	1	0.5	$C_b = \frac{\epsilon_0 b L}{d}$ 5.31×10^{-16}	5.32×10^{-16}	0.18
(b)	0.2	—	0.5	$C_s = \frac{\epsilon_0 h L}{g}$ 6.64×10^{-16}	6.65×10^{-16}	0.15
(c)	0.5	0.5	1	$C = C_b + C_s$ 1.59×10^{-15}	1.60×10^{-15}	0.62

To validate the numerical procedure of computing capacitance, we compute the capacitance for three trivial configurations as shown in Figures 1(a), (b) and (c) which are also mentioned as cases (a), (b) and (c) in Table I. In case (a), a beam of length $L = 30 \mu\text{m}$, width $b = 2 \mu\text{m}$, and thickness $h = 0.5 \mu\text{m}$ is separated from the bottom electrode by a distance $d = 1 \mu\text{m}$. If we consider the surrounding region simply as that between the beam and the bottom electrode, the capacitance is given by $C_b = \epsilon_0 b L / d$. On comparing the numerical value with the value obtained from the analytical

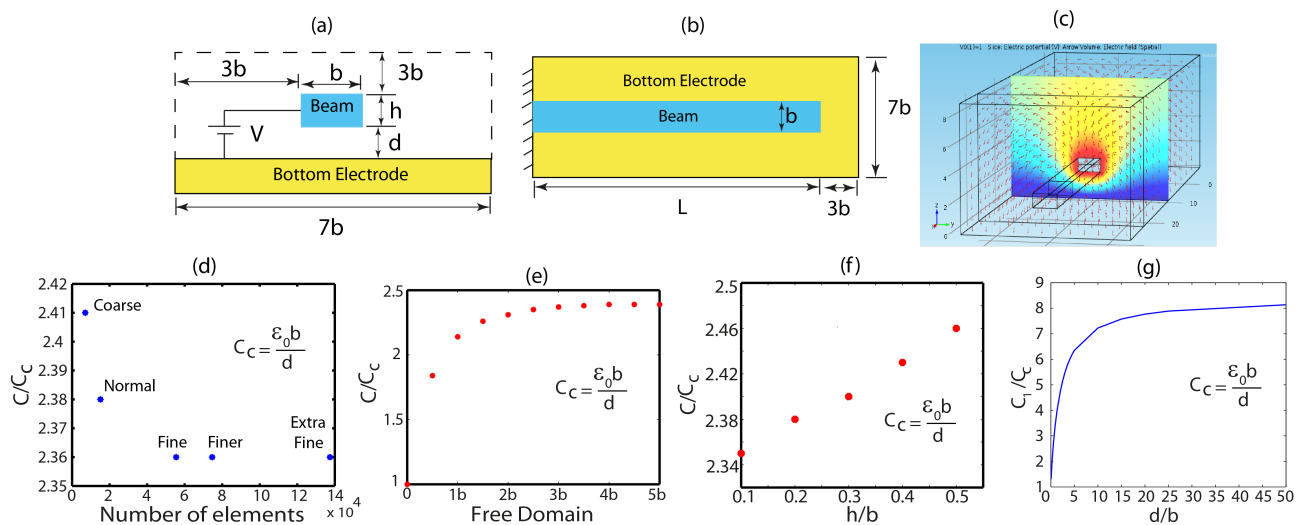


Fig. 2. (a) Front view showing the beam and bottom electrode. (b) Top view of beam and bottom electrode. (c) COMSOL model showing beam, bottom electrode and free space with direct and fringing Electrostatic field distribution. (d) Normalized capacitance versus number of mesh elements. (e) Normalized capacitance versus the free domain. (f) Normalized capacitance versus the normalized thickness, $\frac{h}{b}$ for fixed $b = 2 \mu\text{m}$ such that h is varied from 0.2 to $1 \mu\text{m}$, (g) Normalized capacitance versus normalized gap, $\frac{d}{b}$, for fixed $b = 2 \mu\text{m}$ such that d is varied till $100 \mu\text{m}$.

model, we get a percentage error of less than 1%. Similarly, for the case (b) in which the beam length $L = 30 \mu\text{m}$, width $b = 2 \mu\text{m}$, and thickness $h = 0.5 \mu\text{m}$ is separated from the side electrode by a distance $g = 0.2 \mu\text{m}$, we get a percentage error of less than 1% when compared with the analytical solution $C_s = \epsilon_0 h L / g$. For case (c) in which a beam $L = 30 \mu\text{m}$, width $b = 2 \mu\text{m}$, and thickness $h = 1 \mu\text{m}$ is separated from the bottom electrode by $d = 0.5 \mu\text{m}$ and the side electrode by $g = 0.5 \mu\text{m}$, the percentage error of numerical results with respect to the analytical model, $C = C_b + C_s$, is also found to be under 1%. In the subsequent analysis, we following the same procedure to compute capacitance in rest of the cases as shown in Figure 1.

B. Optimization of the numerical domain

To numerically compute the capacitance in the complex domains as shown in Figures 1(d)-(j), we first optimize the mesh parameters to get the converged solution and then extend the outer boundaries to get invariable value of the capacitance.

For the case shown in Figure 1(d), the beam of length $L = 30 \mu\text{m}$, width $b = 2 \mu\text{m}$, and thickness $h = 0.2 \mu\text{m}$ is separated from the bottom electrode $d = 1 \mu\text{m}$. The side boundaries and top boundary are fixed at a distance $3b$ from the surfaces of the beam as shown in Figures 2(a), (b) and (c). On refining the mesh in the 3D numerical domain from coarse (1×10^4 elements) to extra fine mess (14×10^4 elements), the converged value of capacitance is found at around the fine mesh having $\approx 6 \times 10^4$ elements as shown in Figure 2(d). Figure 2(e) shows the variation of capacitance when the outer boundaries are extended by a distance of b to $5b$. It shows that the capacitance becomes almost invariable when the boundaries are extended beyond a distance of $3b$ to $6b$. Therefore, we extend the outer boundaries in all our analysis by $3b$. Figure 2(f) shows the influence of beam thickness on the capacitance. It shows that as the thickness to width

(for constant width $b = 2 \mu\text{m}$) of the beam increases from 0.1 to 0.5 times, the capacitance ratio increases from 2.35 to 2.46 with a percentage difference of 4%. After optimizing the domain, we obtain the capacitance formula for two different configurations, namely, a beam and the bottom electrode, and a beam and the side electrode, respectively. Subsequently, we propose a generalized formula based on the capacitance of the above two cases and apply it to find the capacitance in an arrays of beams and electrodes.

III. CANTILEVER BEAM AND BOTTOM ELECTRODE

In this section, we obtain the capacitance between a cantilever type of beam and the bottom electrode separated by a distance d as shown in Figure 2(a) and (b). Here, the effect of fringing is also modeled by extending the boundaries of free domain on the side and top portion of the beam. For a beam of length $L = 30 \mu\text{m}$, width $b = 2 \mu\text{m}$, and thickness $h = 0.2 \mu\text{m}$, we numerically obtain the capacitance per unit length C_1 at different values of d/b ratio (varying from 0.03 - 50, for fixed $b = 2 \mu\text{m}$). Figure 2(g) shows the variation of C_1/C_c with d/b ratio, where, $C_c = \frac{\epsilon_0 b}{d}$ is the capacitance per unit length of a parallel plate capacitor without considering the fringing field effects. It shows that C_1 approaches to C_c as d/b approaches to zero and it increases sharply as d/b varies from 0.03 to 20. Over the range of d/b from 20 to 50, the variation of C_1/C_c becomes almost invariable. By finding the numerical fit of the graph as shown in Figure 2(g), we obtain approximate expressions for the capacitance per unit length, C_1 , over the different ranges of d/b ratio as follow:

$$C_1 = [-0.0204 \left(\frac{d}{b}\right)^4 + 0.25 \left(\frac{d}{b}\right)^3 - 1.2 \left(\frac{d}{b}\right)^2 + 3.3 \left(\frac{d}{b}\right) + 1.2] C_c \quad \text{for } 0.03 \leq \frac{d}{b} \leq 4.5$$

$$C_1 = [0.00053 \left(\frac{d}{b}\right)^3 - 0.027 \left(\frac{d}{b}\right)^2 + 0.49 \left(\frac{d}{b}\right) + 4.5] C_c$$

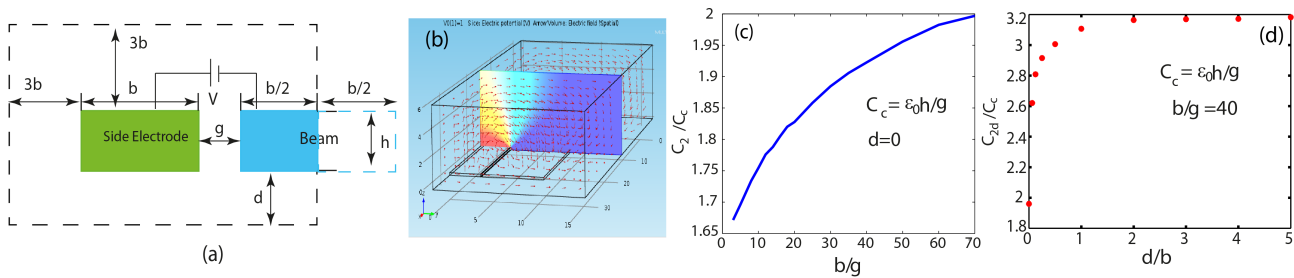


Fig. 3. (a) Front view showing the beam and side electrode. (b) Top view of beam and side electrode. (c) COMSOL model showing beam, side electrode and free space with direct and fringing Electrostatic field distribution. (d) Normalized capacitance versus normalized width, b/g , for fixed $g = 0.1 \mu\text{m}$ such that b is varied from 0.2 to $7 \mu\text{m}$. (e) Normalized capacitance versus normalized bottom gap, d/b , for fixed $b = 4 \mu\text{m}$ such that d is varied from 0 to $20 \mu\text{m}$.

$$C_1 = [8.79 \times 10^{-6} \left(\frac{d}{b}\right)^3 - 0.0013 \left(\frac{d}{b}\right)^2 + 0.069 \left(\frac{d}{b}\right) + 6.835]C_c \quad \text{for } 4.5 \leq \frac{d}{b} \leq 20 \quad (2)$$

where, $C_c = \epsilon_0 b/d$ is the capacitance per unit length without the fringing effects. The corresponding force expressions can be obtained by differentiating the energy stored in the capacitor given by eqn. (2) as follows:

$$F_1 = \left| \frac{\partial U}{\partial d} \right| = \left| \frac{\partial}{\partial d} \left(\frac{1}{2} V^2 C_1 \right) \right|$$

$$F_1 = \frac{1}{2} \frac{\epsilon_0 V^2}{b^3 (d-w)^2} |(-0.0612(d-w)^4 + 0.5(d-w)^3 b - 1.2(d-w)^2 b^2 - 1.2b^4)| \quad \text{for } 0.03 \leq \frac{d}{b} \leq 4.5$$

$$F_1 = \frac{1}{2} \frac{\epsilon_0 V^2}{b^2 (d-w)^2} |(0.001066(d-w)^3 - 0.27(d-w)^2 b - 4.5b^3)| \quad \text{for } 4.5 \leq \frac{d}{b} \leq 20$$

$$F_1 = \frac{1}{2} \frac{\epsilon_0 V^2}{b^2 (d-w)^2} |(0.00001758(d-w)^3 - 0.00013(d-w)^2 b - 6.835b^3)| \quad \text{for } 20 \leq \frac{d}{b} \leq 50 \quad (3)$$

Here, d is replaced by $(d-w)$, where, w is assumed to be the uniform deflection of the beam.

To compare the capacitance per unit length from the proposed formula and the models available in the literature, we take $L = 300 \mu\text{m}$, $b = 20 \mu\text{m}$, $h = 2 \mu\text{m}$, and $d = 8 \mu\text{m}$ [10]. Figure 4(a) shows the comparison of capacitance per unit length versus uniform deflection w of the beam varying from 0 to $7 \mu\text{m}$. It shows that the proposed model given by eqn. (2) gives a percentage error of about 4% to 2% with respect to the numerical result. The empirical model given by Sakurai and Tamaru [9] gives a percentage error of 12% to 4%. The widely used analytical model given by eqn. (1)[4], [5] gives a percentage error of 5% to 32%. The approximate model given by Meijis and Fokemma [19] an error of 11% to 4%. The analytical model based on Schwartz–Christoffel conformal transformation proposed by Chang [14] found to be most accurate model with the fringing effects with a percentage error of 4% to 2%. When we compared the numerical results

with the model without including the fringing effects, i.e., C_c , it gives an error of 55% to 32%. The above comparisons with the numerical results show that the proposed model is valid for large operating range, whereas, the the model proposed by Sakurai and Tamaru [9] is valid for the range $0.03 \leq \frac{d}{b} \leq 3.33$ and $0.03 \leq \frac{d}{h} \leq 3.33$ with a percentage error of 6%. Similarly, we also show the comparison of corresponding electrostatic force per unit length versus deflection for the present model given by eqn. (3), the force based on the model by Sakurai and Tamaru [9], the model used by Dumitru [10], and the model without fringing effects. All the models give similar variation with the deflection.

IV. CANTILEVER BEAM AND SIDE ELECTRODE

In this section, we take a beam of length $L = 30 \mu\text{m}$, thickness $h = 0.2 \mu\text{m}$, and width b , which is separated from the side electrode by distance $g = 0.1 \mu\text{m}$ as shown in Figure 3(a) and (b). Since most of the planar structure are placed closer to the substrate, we subdivide this case into two cases. In the first case, we consider direct effect and the fringing field effects from the top and the side domains but neglect the effect from the bottom. Such cases are obtained by taking $d = 0$ in Figure 3(a). In the second case, we vary d to capture the additional fringing effects due to the gap between the beam and the bottom substrate. Following the same numerical procedure as mentioned in the previous section, we make a model as shown in Figure 3(b) in which the numerical domain is defined by taking half of the beam width, the side electrode and extended top and side boundaries. Subsequently, we obtain the numerical results as shown Figures 3(c) and (d) for the two cases, respectively. It is also observed that by taking half of the beam width, the percentage error of the capacitance with respect to that by taking full beam width and the extended boundary does not go beyond 1.5%.

Figure 3(c) shows the variation of capacitance per unit length, C_2 , with b/g ratio varying from 5 to 70 for the first case under which $d = 0$. The numerical fit of the results can be captured by the following expression over the different range of b/g ratios as follow

$$C_2 = \left[1.13 \times 10^{-6} \left(\frac{b}{g}\right)^3 - 0.00019 \left(\frac{b}{g}\right)^2 + 0.013 \left(\frac{b}{g}\right) \right]$$

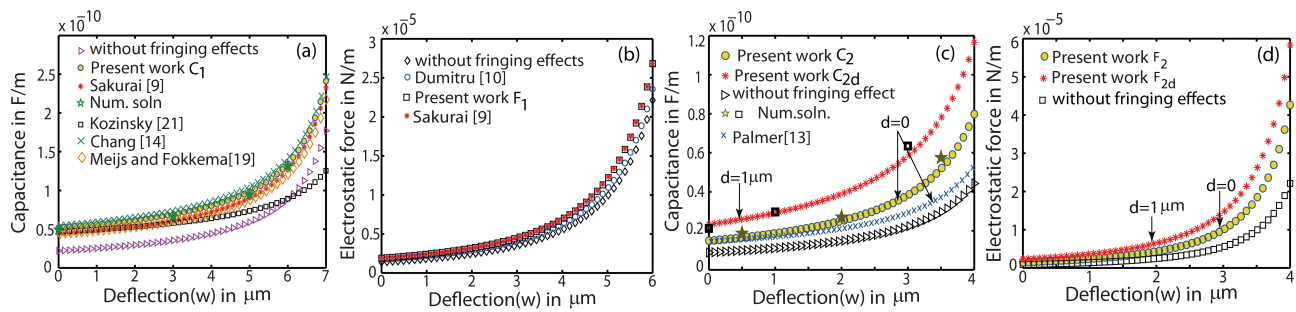


Fig. 4. (a) Comparison of capacitance/unit length versus deflection (w) between present expression C_1 , Sakurai [9], Kozinsky [5], Chang [14], Meijis and Fokemma [19], the expression without fringing effects with the numerical solution. (b) Comparison of electrostatic force versus deflection (w) between the present work, F_1 , Dumitru [10], Sakurai [9] and the expression without fringing effects for $d = 8\mu\text{m}$, $b = 20\mu\text{m}$, $h = 2\mu\text{m}$, $\epsilon_0 = 8.854 \times 10^{-12}$ F/m. [10]. (c) Comparison of capacitance/unit length versus deflection (w) between the present expression C_2 , Palmer [13] and the expression without fringing effect with the numerical solution for $d = 0$. The comparison between the present expression C_{2d} with the numerical solution for $d = 1\mu\text{m}$ is also shown. (d) Comparison of electrostatic force versus deflection (w) between present expression F_2 , F_{2d} and the expression without fringing effects for values $b = 16\mu\text{m}$, $g = 5\mu\text{m}$, $h = 5\mu\text{m}$, $\epsilon_0 = 8.854 \times 10^{-12}$ F/m. [11].

$$+ 1.638 \left] C_{c1} \quad \text{for } 2 \leq \frac{b}{g} \leq 70 \text{ \& } d = 0, \quad (4) \quad -0.44 \left(\frac{d}{b} \right) - 2.83 \left| \quad \text{for } 0.25 \leq \frac{d}{b} \leq 5 \quad (6)$$

where, $C_{c1} = \epsilon_0 h/g$ is the capacitance per unit length without the fringing effects. Similarly, Figure 3(d) shows the variation of capacitance per unit length, C_{2d} , with d/b ratio varying from 0 to 5 for $b/g = 40$. The corresponding numerical fit is given by the formula

$$C_{2d} = \left[100 \left(\frac{d}{b} \right)^3 - 57 \left(\frac{d}{b} \right)^2 + 11 \left(\frac{d}{b} \right) + 2.145 \right] C_{c1} \quad \text{for } 0 \leq \frac{d}{b} \leq 0.25$$

$$C_{2d} = \left[-0.00316 \left(\frac{d}{b} \right)^4 + 0.043 \left(\frac{d}{b} \right)^3 - 0.21 \left(\frac{d}{b} \right)^2 + 0.44 \left(\frac{d}{b} \right) + 2.83 \right] C_{c1} \quad \text{for } 0.25 \leq \frac{d}{b} \leq 5 \quad (5)$$

For $d/b > 5$, $C_{2d} \approx 3.18C_{c1}$. Finally, a case in which d is sufficiently large such that the fringing fields effects in the top as well as the bottom portion become similar, the capacitance per unit length can be obtained by $(2C_2 - C_{c1})$ with a percentage error of about 7% with respect to the numerical results.

Like the previous case, the force expression can be obtained by differentiating the energy stored in a capacitor given by eqn. (4) and (5), respectively.

$$F_2 = \frac{1}{2} \frac{\epsilon_0 V^2 h}{(g-w)^5} \left| (-4.52 \times 10^{-6} b^3 + 5.7 \times 10^{-4} b^2 (g-w) - 0.026b(g-w)^2 - 1.638(g-w)^3) \right| \quad \text{for } 2 \leq \frac{b}{g} \leq 70 \text{ \& } d = 0$$

$$F_{2d} = \frac{1}{2} \frac{\epsilon_0 V^2 h}{(g-w)^2} \left| -100 \left(\frac{d}{b} \right)^3 + 57 \left(\frac{d}{b} \right)^2 - 11 \left(\frac{d}{b} \right) - 2.145 \right| \quad \text{for } 0 \leq \frac{d}{b} \leq 0.25$$

$$F_{2d} = \frac{1}{2} \frac{\epsilon_0 V^2 h}{(g-w)^2} \left| 0.00316 \left(\frac{d}{b} \right)^4 - 0.043 \left(\frac{d}{b} \right)^3 + 0.21 \left(\frac{d}{b} \right)^2 \right|$$

Here, w is the deflection of the beam with respect to a given g .

Figure. 4(c) shows the variation of the capacitance per unit length versus deflection, w , obtained from the proposed model given by eqn. (4) when $d=0$ for the configuration having $L = 150 \mu\text{m}$, $h = 5 \mu\text{m}$, $b = 16 \mu\text{m}$, and $g = 5 \mu\text{m}$ [11]. On comparing it with the numerical results, it is found that the proposed expression gives a percentage error of 3% to 5% when w is varied from 0 to 4. We compared the analytical model based on Schwartz–Christoffel conformal transformation proposed by Palmer [13] with numerical solutions (for $d = 0$) it gives an error of 8% to 36%. We also compare the empirical model given by eqn. (5) for non-zero value of $d = 1 \mu\text{m}$ with the numerical results. The percentage error is found to be about 4% to 7%. When we compare the numerical results with the analytical model without the fringing effects for the case of $d = 0$, it gives an error of about 48%. Since, Sakurai and Tamaru model [9] is not valid for finding capacitance under the given condition, we have not compared its value with the present model. Similarly, Figure 4(d) shows the comparison of electrostatic force per unit length versus deflection for $d = 0$ and $d = 1$ using eqn. (6). We also compare the variation of the forces without considering the fringing field effects. All the models vary similarly, however, with different magnitudes. Finally, it is to be noted that the model presented in this section is unique in capturing the fringing field effect when a configuration consisting of a beam and side electrode is considered.

V. APPLICATION TO AN ARRAY OF BEAMS AND ELECTRODES

In this section, we discuss the application of above models in evaluating the capacitance in an array of beams and electrodes. In the first case, we take different combination of beams and side electrodes. In the second case, we consider different configurations consisting of beams, side electrodes and bottom electrode.

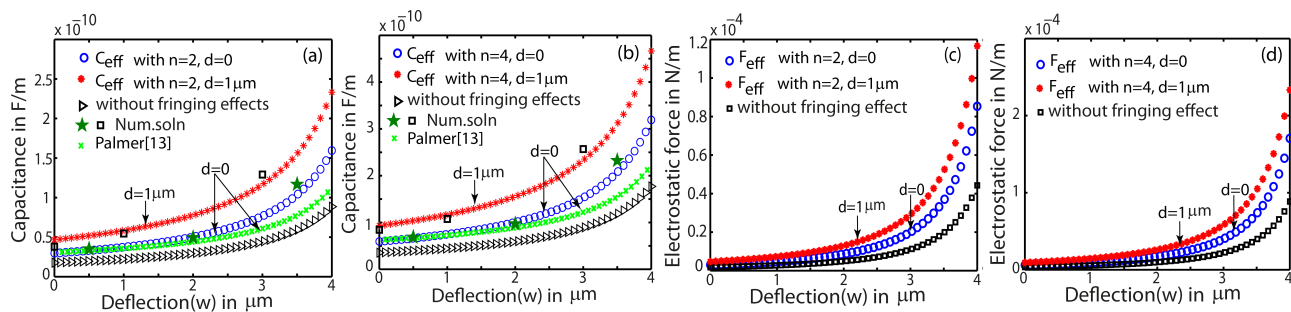


Fig. 5. Comparison of capacitance/unit length versus deflection (w) between the present expression $C_{\text{eff}} = nC_2$, the expression without fringing effects and Palmer [13] with the numerical results for $d = 0$. We also present the comparison between the present expression $C_{\text{eff}} = nC_{2d}$ and the numerical solution for $d = 1 \mu\text{m}$ when (a) $n = 2$ and (b) $n = 4$. Comparison of the corresponding electrostatic force versus deflection (w) between present expression $F_{\text{eff}} = nF_2(d = 0)$, $F_{\text{eff}} = nF_{2d}(d = 1 \mu\text{m})$ and the expression without fringing effects ($d = 0$) for (c) $n = 2$ and (d) $n = 4$. The other dimensions are taken as $b = 16 \mu\text{m}$, $g = 5 \mu\text{m}$, $h = 5 \mu\text{m}$, $\epsilon_0 = 8.854 \times 10^{-12} \text{ F/m}$. [11].

A. Array of beams and side electrodes

In this case, different configurations are formed by taking different arrangements of beam and electrodes as shown in Figure 1(f) and (g), respectively. In Figure 1(f), a beam is separated by two side electrodes by a distance g on each side. For a case of $d=0$ in which the fringing field effects from the bottom electrode is negligible, the electric field lines are symmetric about the line passing through the middle of the beam width. Since C_2 is the capacitance per unit length for the configuration (see Figure 3(a)) in which half of the beam width and the full side electrode is considered, the total capacitance per unit length for the present case as shown in Figure 1(f) is twice the value of C_2 , i.e., $2C_2$. Similarly, the capacitance per unit length for the case shown in Figure 1(g) in which two beams and three electrodes are found based on the two different patterns of electric field lines as shown in the upper portion of Figure 7(c). In one of the patterns, the electric field lines are similar to the previous case for the beam and the side electrode located at the ends. In this case, for the two end effects, the total capacitance per unit length is given by $2C_2$. In another pattern, the field lines are reduced and they form similar types of patterns for the combination of beam and side electrode located in the middle. In this case, the total capacitance per unit length is given by $2(1 - \gamma)C_2$, where γ is the correction factor to capture reduced C for the inner beams and electrodes, respectively. However, on comparing the results with the numerical results, the factor γ is found to be negligibly small. For n number of beam and electrode combinations, the effective capacitance per unit length can be given by $C_{\text{eff}} = 2C_2 + (n - 2)(1 - \gamma)C_2 = 4C_2$. Similarly, the effective force can also be written as $F_{\text{eff}} = 2F_2 + (n - 2)(1 - \gamma)F_2 = 4F_2$.

Figure 5(a) and (b) shows the variation of the capacitance per unit length versus the beam deflection, w obtained from the above relation and Palmer [13] when $d = 0$ for $n=2$ and 4 . We also compare our model with the numerical result when $d = 1 \mu\text{m}$ for $n=2$ and 4 . On comparing the results from the present models with the numerical values, we find the percentage error of about 8% for both the cases. We also found that model from Palmer [13] can also be used in this case for small w . When we compute the capacitance based

on the model without considering the fringing field effects, the percentage error is found to be about 50% with respect to the numerical results. Similarly, we show the variation of forces with the uniform beam deflection w for $n=2$ and 4 in Figure 5(c), and (d), respectively, with and without fringing field effects.

B. Array of beams, side electrodes and bottom electrode

In this section, we apply the formulation developed in the previous section to find the capacitance per unit length in different configurations consist of beams, side electrodes and the bottom electrode as shown in Figures 1(h), (i) and (j). Such configurations are very important from the point that they are commonly found in the literature [2], [3]. When we compute the capacitance per unit length for the combination of a beam, a side and a bottom electrode as shown in Figure 1(h), a very approximate value can be obtained from $C_1 + C_2$. However, if we observe the actual field lines in the combination as shown in Figure 6(d) and compare the field lines in the individual cases of C_1 and C_2 as shown in Figures 6(a) and (b), respectively, the value of $C_1 + C_2$ as shown in Figure 6(c) tends to give more value than the actual as observed in Figure 6(d). Therefore, we introduce a correction factor ζ such that the effective capacitance per unit length can be written as $C_{\text{eff}} = (C_1/2 + C_2)(1 - \zeta) + C_1/2$, where, ζ is given by $\zeta = 0.00075 \left(\frac{d}{g}\right)^2 - 0.025 \left(\frac{d}{g}\right) + 0.32$. When we compare the capacitance obtained from this model with the numerical result as shown in Figure 8(a), we get an error of about 1 to 4%. On the other hand, Sakurai and Tamaru model [9] which is valid for this case overpredicts the value from 3% to 34% as the distance between the beam and the bottom electrode reduces. However, when we use the combined model of Palmer [13] and Chang [14], it gives an error of 4 to 14%. In the case, the model without considering the fringing effect under predicts the value with an error of about 50%. Similarly, we find the capacitance per unit length when a beam is separated from the two side electrodes and a bottom electrode as shown in Figure 7(b). Under this condition, the electric field lines as shown in Figure 7(a) and (b) show that the effective capacitance can be obtained from $C_{\text{eff}} = 2(C_1/2 + C_2)(1 - \zeta)$. On comparing

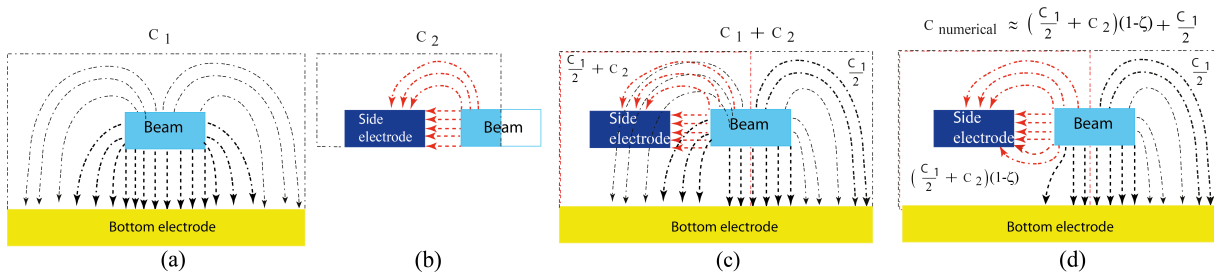


Fig. 6. Electric field lines showing direct and fringing effects in the configuration consisting of (a) a beam and extended bottom electrode (C_1); (b) a beam and a side electrode (C_2); and a beam, side electrode and a bottom electrode (c) when (a) and (b) are added together ($C_1 + C_2$) and (d) under the actual condition.

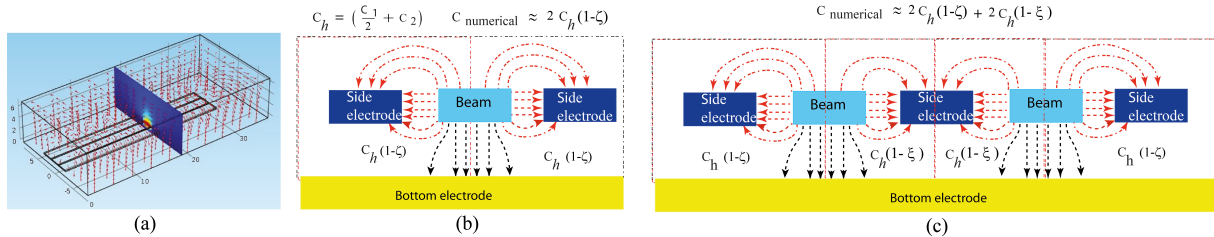


Fig. 7. (a) Numerically computed electric field lines showing the direct and fringing effects in an array of beams, side electrode and the bottom electrode. Similar electric field can be described in an array of (b) one beam, two side electrodes and a bottom electrode; and (c) two beams, three side electrodes and a bottom electrode.

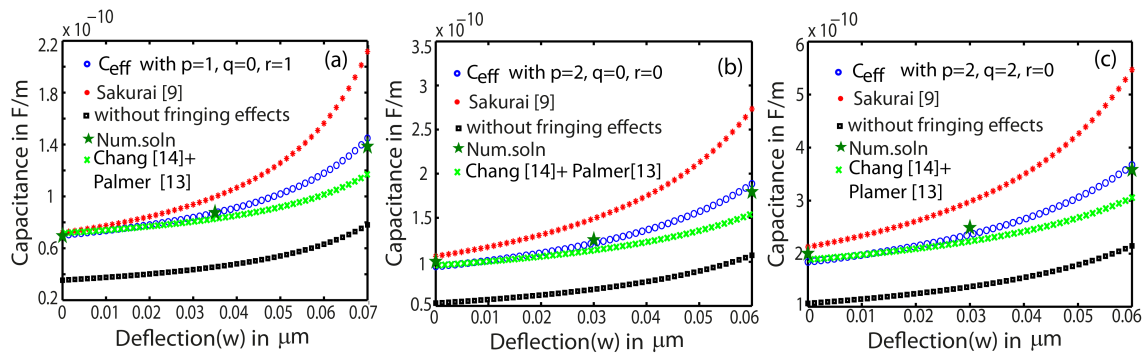


Fig. 8. Comparison of capacitance per unit length versus deflection (w) between present expression C_{eff} , Sakurai [9], combined model of Palmer [13] and Chang [14], and the expression without fringing effect with the numerical solution when (a) $p = 1, q = 0, r = 1$; (b) $p = 2, q = 0, r = 0$; and (c) $p = 2, q = 2, r = 0$; for $d = 1\mu\text{m}, b = 2\mu\text{m}, g = 0.1\mu\text{m}, h = 0.2\mu\text{m}, \epsilon_0 = 8.854 \times 10^{-12} \text{ F/m}$.

the values obtained from the model with the numerical results as shown in Figure 8(b), we get a percentage error of about 6%. While the values from Sakurai and Tamaru model [9] gives a percentage error of about 35% and the combined model of Palmer [13] and Chang [14] gives an error of 4 to 14%, the model without the fringing effects under predict the values with about 50% error.

To compute the capacitance per unit length in a configuration which consists of two beams, three side electrodes and a bottom electrode, the electric field lines can be observed in different regions as shown in Figure 7(c). Like the previous section, the effective capacitance in the inner portion is less than that of the outer region. While the two outer region show the similar type of electric lines, the inner portion show the reduced effect which is captured by another correction factor ξ . Therefore, the effective capacitance per unit length can be obtained from $C_{\text{eff}} = 2C_h(1 - \zeta) + 2C_h(1 - \xi)$, where, $C_h = (C_1/2 + C_2)$ and $\xi = 1.3\zeta$. On comparing the values

obtained from the model with the numerical results as shown in Figure 8(c), we get an error of about 6%. However, the values from Sakurai and Tamaru model [9] gives a percentage error of about 35%, the combined model of Palmer [13] and Chang [14] gives an error of 4 to 14%, the model without fringing effects give the values of about 45% error. It shows that the model can be generalized for an array of many beams and side electrodes with the bottom electrode as follow

$$C_{\text{eff}} = p \left(\frac{C_1}{2} + C_2 \right) (1 - \zeta) + q \left(\frac{C_1}{2} + C_2 \right) (1 - \xi) + r \frac{C_1}{2}$$

where, p - represents the end effect and takes a value of either 1 for even number of beam and side electrode combination or 2 for odd number of beam and side electrode combination, q - represents the number of inner beam and side electrode combinations, r - also represent the end effects but it take a value of 0 for odd number of beam and side electrode combination or 1 for even number of beam and side electrodes.

Similarly, the generalized form of the electrostatic force can be written as

$$F_{\text{eff}} = p \left(\frac{F_1}{2} + F_2 \right) (1-\zeta) + q \left(\frac{F_1}{2} + F_2 \right) (1-\xi) + r \frac{F_1}{2}.$$

Figure 8(a), (b) and (c) show the variation of electrostatic force with the uniform beam displacement for the configurations represented by $(p = 1, q = 0, r = 1)$, $(p = 2, q = 0, r = 0)$, and $(p = 2, q = 2, r = 0)$ as shown in Figure 6(d), Figures 7(b) and (c), respectively. On comparing its value with other models, we find that Sakurai and Tamaru model [9] over predicts the value and the model without the fringing effects under predicts it in all the cases.

Finally, we state that we systematically obtained approximate model for computing the capacitance as well force in different configurations of beam and electrodes. Although the proposed models have been compared with the numerical results for many different cases under a wide operating range, their application outside the given range may give some erroneous results. Nevertheless, the effectiveness of the proposed model can be observed from its application in an array of beams and electrodes.

VI. CONCLUSION

In this work, we have proposed models for computing capacitance and forces based on the numerical results in simple as well as complex configurations of beams and electrodes. We first validate our numerical approach with the standard formula and then optimize the numerical domain in terms of outer boundaries and number of elements for computing capacitance in the non-trivial configurations. Subsequently, we obtain approximate formulas for two important conditions, namely, a beam and an extended bottom electrode, and a beam and the side electrode. These formulas approximate the numerical values with percentage error of about 2% to 8%. Finally, we apply these formulas accordingly to evaluate the capacitance per unit length in an array of beam, side electrodes and bottom electrode. We found a maximum percentage error of about 6% with respect to the numerically obtained value. Based on the proposed formula of capacitance per unit length, we have also obtained the expression for the electrostatic forces in all the configurations. On comparing the numerical results with the model without the fringing field effects, the error is found to be about 50%. Therefore, we conclude that we have demonstrated the application of simple formulas based on direct and fringing field effects to compute forces in different systems.

REFERENCES

- [1] P. N. Kambali and A. K. Pandey, "Nonlinear response of a microbeam under combined direct and fringing field excitation", *ASME J. of Comp. and Nonlin. Dyn.*, vol. 10, pp. 051010-10, 2015.
- [2] P. N. Kambali, G. Swain, A. K. Pandey, E. Buks, and O. Gottlieb, "Coupling and tuning of modal frequencies in DC biased MEMS arrays," *Appl. Phys. Lett.*, vol. 107, pp. 063104-4, 2015.
- [3] A. Isacsson, and J. M. Kinaret, "Parametric Resonances in Electrostatically Interacting Carbon Nanotube Arrays", *Phys.Rev.B*, vol. 79, pp. 165418-165429, 2008.
- [4] B. I. Bleaney, and B. Bleaney, *Electricity and Magnetism*. Oxford University Press, New York, 1989.

- [5] I. Kozinsky, H. W. Ch. Postma, I. Bargatin and M. L. Roukes, Tuning nonlinearity, dynamic range, and frequency of nanomechanical resonators, *Appl. Phys. Lett.*, vol. 88, pp. 253101-3, 2006.
- [6] A. H. Nayfeh, M. I. Younis, and E. M. Abdel-Rahman, "Dynamic Pull-in Phenomenon in MEMS Resonators", *Nonlinear Dyn.*, vol. 48, pp. 153-163, 2007.
- [7] S. Gutschmidt, and O. Gottlieb, "Nonlinear Dynamic Behavior of a Microbeam Array subject to Parametric Actuation at Low, Medium and Large DC-voltages", *Nonlinear Dyn.*, vol.67, pp. 1-36, 2012.
- [8] Y. C. Hu, and C. S. Wei, "An Analytical Model Considering the Fringing Fields for Calculating the Pull-in Voltage of Micro Curled Cantilever Beams", *J. Micromech. Microeng.*, vol. 17, pp. 61-67, 2007.
- [9] T. Sakurai, and K. Tamaru, "Simple Formulas for Two- and Three Dimensional Capacitances", *IEEE Transactions on Electron Devices*, vol. 2, pp. 183-185, 1983.
- [10] I. Dumitru, M. Israel and W. Martin, "Reduced Order Model Analysis of Frequency Response of Alternating Current Near Half Natural Frequency Electrostatically Actuated MEMS Cantilevers", *J. Comp. Non. Dyn.*, vol. 8, pp. 031011-031015, 2013.
- [11] Y. Linzon, B. Ilic, L. Stella and K. Slava, "Efficient Parametric Excitation of Silicon-on-Insulator Microcantilever Beams by Fringing Electrostatic Fields", *J. Appl. Phys.*, vol. 113, pp. 163508-163519, 2013.
- [12] <http://www.intellisense.com/>.
- [13] H. B. Palmer, "Capacitance of a Parallel-Plate Capacitor by the Schwartz-Christoffel Transformation", *Trans. AIEE*, Vol. 56, pp. 363, March 1927.
- [14] W. H. Chang, "Analytic IC-Metal-Line Capacitance Formulas," *IEEE Trans. Microwave Theory Tech.*, Vol. MTT-24, pp. 608-611, 1976; also vol. MTT-25, p. 712, 1977.
- [15] C. P. Yuan and T. N. Trick, "A Simple Formula for the Estimation of the Capacitance of Two-Dimensional Interconnects in VLSI Circuits", *IEEE Electron Device Lett.*, Vol. EDL-3, pp. 391-393, 1982.
- [16] M. Hosseini, G. Zhu, and Y. Peter, "A New Formulation of Fringing Capacitance and its Application to the Control of Parallel-Plate Electrostatic Micro Actuators", *Analog Integr Circ Sig Process*, vol. 53, pp. 119128, 2007.
- [17] W. C. Chew, and J. A. Kong, "Effects of Fringing Fields on the Capacitance of Circular Microstrip Disk", *IEEE Trans. Microwave Theory Tech*, vol. 2, pp. 98-104, 1980.
- [18] G. J. Slogget, N. G. Barton, and S. J. Spencer, "Fringing Fields in Disc Capacitors", *J. Phys. A*, vol. 19, pp. 2725-2736, 1986.
- [19] V. Leus and D. Elata, "Fringing Field Effect in Electrostatic Actuators", *Technical Report ETR*, 2004.
- [20] <http://www.comsol.co.in/comsol-multiphysics>



Prashant N. Kambali received the B.E. degree in Mechanical Engineering in 2007 and M.Tech. in Machine Design in 2009 from the Basaveshwar Engineering College, Bagalkot, Karnataka, India. He is currently working toward the Ph.D. degree in Dept. of Mechanical and Aerospace Engineering, Indian Institute of Technology Hyderabad, Kandi, India. His research interests include nonlinear dynamics, MEMS, NEMS.



Ashok K. Pandey received the B.E. degree in mechanical engineering from Bhilai Institute of Technology, Durg, India, in 2001, and the M.S. and Ph.D. degrees in mechanical engineering from Indian Institute of Science, Bengaluru, India, in 2003 and 2007 respectively.

Currently, he is an Assistant Professor in Department of Mechanical and Aerospace Engineering, Indian Institute of Technology, Hyderabad, India. His research interest includes nonlinear dynamics, vehicle dynamics and micro and nanomechanics.